Geophysical Journal International

Geophys. J. Int. (2019) **219,** 1365–1376
Advance Access publication 2019 August 19
GJI Heat Flow and Volcanology

doi: 10.1093/gji/ggz374

Estimating plume heights of explosive eruptions using high-frequency seismic amplitudes

Azusa Mori and Hiroyuki Kumagai

Graduate School of Environmental Studies, Nagoya University, Nagoya, Aichi 464-8601, Japan. E-mail: mori.azusa@j.mbox.nagoya-u.ac.jp

Accepted 2019 August 18. Received 2019 July 23; in original form 2018 November 28

SUMMARY

Seismic signals during explosive eruptions have been correlated to eruption size or eruption volume flux for individual eruptive episodes. However, the universality of these correlations has yet to be confirmed. We quantified the sources of high-frequency seismic signals associated with sub-Plinian and Vulcanian eruptions at Kirishima (Japan), Tungurahua (Ecuador) and other volcanoes in Japan using a simple approach based on highly scattered seismic waveform characteristics. We found that eruption plume heights scale to seismic source amplitudes and are described by two relations depending on the value of source amplitudes: power-law and exponential relations for plume height >6 km and <6 km, respectively. Though conceptually similar, our scaling relations differ from the previously proposed relation based on reduced displacement. By comparing seismic and geodetic data during sub-Plinian eruptions at Kirishima, we found that the source amplitude is proportional to eruption volume flux. Combining these relations, we show that our scaling relation for Plinian eruptions is consistent with predictions from plume dynamics models. We present a source model to explain the proportionality between the source amplitude and eruption volume flux assuming a vertical crack or a cylindrical conduit as the source. The source amplitude can be estimated in seconds without any complicated data processing, whereas eruption plumes take minutes to reach their maximum heights. Our results suggest that high-frequency seismic source amplitudes are useful for estimating plume heights in real time.

Key words: Explosive volcanism; Remote sensing of volcanoes; Volcano monitoring; Volcano seismology.

1 INTRODUCTION

Seismic observations, which are widely used to monitor active volcanoes (e.g. Chouet & Matoza 2013), have revealed that two main types of seismic signals are common during explosive eruptions: eruption tremor and explosion events (Fig. 1). Eruption tremor exhibits sustained oscillatory signatures during steady Plinian-type eruptions, and explosion events show isolated waveforms generated by discrete Vulcanian-type eruptions. The correlation between seismic amplitudes and eruption size or eruption volume flux has been investigated by using recent eruption data at various volcanoes. At Piton de la Fournaise, erupted lava volume was correlated to cumulative quadratic source amplitudes for eruption tremor signals below 5 Hz (Battaglia *et al.* 2005). Cumulative source amplitudes in 5–10 Hz were correlated to eruption volume at Tungurahua, Ecuador (Kumagai *et al.* 2015). Correlations between the ash fallout mass and cumulative quadratic median amplitudes of eruption tremor in the 0.5–5 Hz band were found for each phase of the 2015 eruption at Cotopaxi, Ecuador (Bernard *et al.* 2016). For the 2011 sub-Plinian eruptions at Kirishima, Japan, the linear relation between seismic power amplitudes in the 1–7 Hz band and eruption volume flux was observed during quasi-stable or slowly growing eruption phases (Ichihara 2016). At Pavlof volcano, Alaska, plume heights were correlated to seismic amplitudes in the 0.8–5 Hz band during waxing and waning eruption phases, respectively (Fee *et al.* 2017). Plume heights during the 2008 eruption at Kasatochi volcano (Aleutian Islands) and the 2006 eruption at Augustine (Alaska) were inferred from the relation between eruption rates and far-field seismic amplitudes assuming a single force source (Prejean & Brodsky 2011). Although various correlations have been indicated, the universality of them has yet to be confirmed. A systematic approach to quantify the sources of eruption tremor and explosion events is required to compare seismic signals associated with eruptions at different volcanoes. Reduced displacement D_R is a normalized measure of amplitude (Aki & Koyanagi 1981) and used to express the size of tremor. McNutt (1994, 2004) investigated the relationship between D_R and the volcanic explosivity index (VEI; Newhall & Self 1982), but reported a wide range of D_R values for each

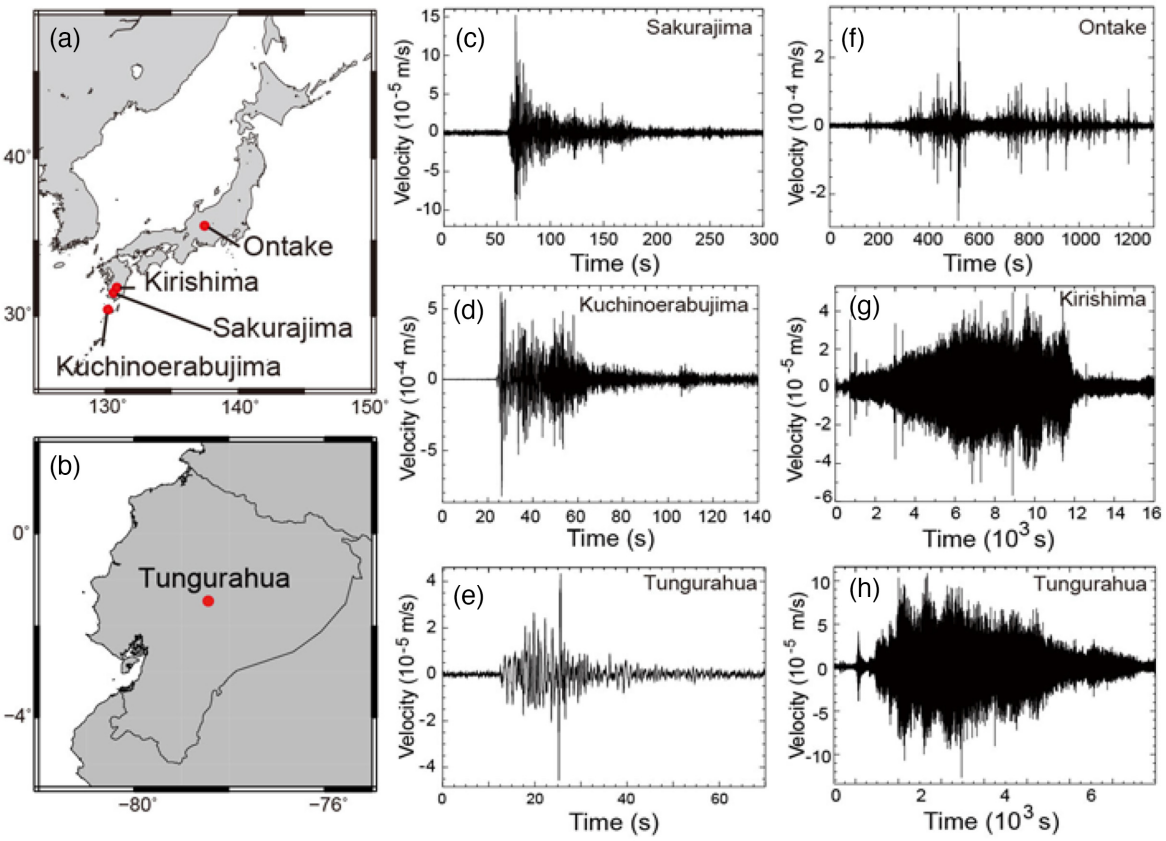

Figure 1. Eruption tremors and explosions at various volcanoes. (a and b) Locations of volcanoes in Japan and Ecuador, respectively. (c–e) Explosion events observed during Vulcanian eruptions at Sakurajima, Kuchinoerabujima and Tungurahua, respectively. (f–h) Tremors observed during a phreatic eruption at Ontake and during sub-Plinian eruptions at Kirishima and Tungurahua, respectively. These seismic signals were recorded at stations in local networks deployed at the individual volcanoes (see Fig. 3).

VEI rank. McNutt (1994) also indicated that D_R is related to plume height, but this relation has not been systematically examined using recent eruption data.

Volcanoes have highly heterogeneous structures characterized by the mean free path, which represents the average travel distance of seismic waves between scatterers (Sato *et al.* 2012). In such structures, wavefields are dominated by multiple scattering in high-frequency bands, resulting in isotropic *S*-wave radiation patterns (Kumagai *et al.* 2010; Morioka *et al.* 2017). Based on the assumption of isotropic *S* wave in a high-frequency band around 5–10 Hz, the amplitude source location (ASL) method was developed (Battaglia & Aki 2003; Kumagai *et al.* 2010). This method estimates the source location and source amplitude by a grid search using seismic amplitudes of various volcano-seismic signals (Battaglia *et al.* 2003, 2005; Kumagai *et al.* 2010, 2011, 2013, 2014, 2015; Ogiso & Yomogida 2012, 2015; Ogiso *et al.* 2015; Kurokawa *et al.* 2016; Ichimura *et al.* 2018). It is thus possible to quantify the seismic source amplitude without information about the source mechanism by using seismic signals in the 5–10 Hz band. Kumagai *et al.* (2013) found a proportional relation between seismic magnitude and the logarithm of the source amplitude for volcano-tectonic earthquakes and long-period and explosion events at various volcanoes, indicating that the source amplitude can be used as a quantitative measure of event size.

In this study, we estimated the source amplitudes of eruption tremors and explosion events observed during recent eruptions at Sakurajima, Kuchinoerabujima, Kirishima and Ontake in Japan and Tungurahua in Ecuador (Fig. 1) and compared the source amplitudes with eruption plume heights and eruption volume fluxes. Our results indicate that plume heights of explosive eruptions scale to the source amplitude, which is proportional to eruption volume flux. We theoretically derive the proportional relation between the source amplitude and eruption volume flux by using a moment tensor source model based on the theory of seismic source equivalents (Haney *et al.* 2018). We then show that our scaling relation for Plinian-type eruptions is consistent with predictions of plume dynamics models. These results suggest that our simple source quantification approach is useful for estimating eruption plume heights and contributes to a better understanding of eruptive processes.

2 METHODS AND DATA

2.1 Estimation of the source amplitude and cumulative source amplitude

We estimated the source amplitude (A_s, $m^2\ s^{-1}$) and cumulative source amplitude (I_s, m^2) for eruption tremors and explosion events following the method of Kumagai *et al.* (2015) in which isotropic *S*-wave radiation is assumed for high-frequency (5–10 Hz) seismograms. Previous studies adopting this assumption have successfully applied the ASL method to seismograms in this frequency band (e.g. Battaglia & Aki 2003; Kumagai *et al.* 2010; Ogiso & Yomogida 2012; Ichimura *et al.* 2018), and the method has also been validated by the theoretical study of Morioka *et al.* (2017) based on numerical

waveform simulations using realistic heterogeneous volcano structures with intrinsic attenuation and topography. The band-passed (centre frequency f) ground velocity v_i at the ith station may be written as

$$v_i(t+\tau_i) = A_0 s_0(t)\frac{e^{-C\tau_i}}{r_i}, \quad (1)$$

where t is time, A_0 and s_0 are the S-wave radiation coefficient and the second time derivative of the moment function, respectively, τ_i and r_i are the S-wave traveltime and source-station distance at the ith station, respectively, and $C = \pi f/Q$, where Q is medium attenuation. We used a sliding time window t_s^k defined as

$$t_s^k = t_s + (k-1)T_w, \quad (k = 1, 2, 3, \ldots), \quad (2)$$

where t_s is the source origin time and T_w is the window duration. We define $\tilde{v}_i$ as the envelope of v_i and w_i as $\tilde{v}_i$ averaged over the time window T_w, which is given as

$$w_i(t_s^k + \tau_i) = \frac{1}{T_w}\int_0^{T_w} \tilde{v}_i(t + t_s^k + \tau_i)\mathrm{d}t = A_s^k \frac{\mathrm{e}^{-C\tau_i}}{r_i}, \quad (3)$$

where

$$A_s^k = \frac{A_0}{T_w}\int_0^{T_w} \tilde{s}_0(t + t_s^k)\mathrm{d}t. \quad (4)$$

Here, A_s^k is the source amplitude at source time t_s^k and $\tilde{s}_0$ is the envelope of s_0. The discrete forms of eqs (3) and (4) are

$$w_i(t_s^k + \tau_i) = \frac{1}{L_w}\sum_{l=0}^{L_w-1} \tilde{v}_i(l\Delta t + t_s^k + \tau_i) \quad (5)$$

and

$$A_s^k = \frac{A_0}{L_w}\sum_{l=0}^{L_w-1} \tilde{s}_0(l\Delta t + t_s^k), \quad (6)$$

where Δt is the sampling interval and $T_w = L_w\,\Delta t$. We estimate A_s^k in the kth time window as

$$A_s^k = \frac{1}{N}\sum_{i=1}^{N} w_i^o(t_s^k + \tau_i) r_i \mathrm{e}^{C\tau_i}, \quad (7)$$

where N is the number of stations. Here, w_i^o is the observed velocity envelope amplitude averaged over the time window T_w at the ith station:

$$\begin{aligned} w_i^o(t_s^k + \tau_i) &= \frac{1}{T_w}\int_0^{T_w} \tilde{v}_i^o(t + t_s^k + \tau_i)\mathrm{d}t, \\ &= \frac{1}{L_w}\sum_{l=0}^{L_w-1} \tilde{v}_i^o(l\Delta t + t_s^k + \tau_i), \end{aligned} \quad (8)$$

where $\tilde{v}_i^o(t)$ is the envelope of the observed vertical velocity waveform. We identify the maximum A_s^k in sliding time windows during each eruption tremor or explosion event and regard this maximum A_s^k as the source amplitude A_s.

We define the cumulative source amplitude I_s as

$$\begin{aligned} I_s &= \frac{1}{N}\sum_{i=1}^{N}\int_0^{T} \tilde{v}_i^o(t) r_i \mathrm{e}^{C\tau_i}\mathrm{d}t, \\ &= \frac{T}{NL}\sum_{i=1}^{N}\sum_{l=0}^{L-1} \tilde{v}_i^o(l\Delta t) r_i \mathrm{e}^{C\tau_i}, \end{aligned} \quad (9)$$

where $T = L\Delta t$ is the tremor or event duration (Fig. 2). We used $T_w = 10$ s, a constant S-wave velocity (β) of 1400 m s^{-1} and $Q = 60$ following Kumagai *et al.* (2015). Because Q values of around 60 have been estimated at various volcanoes (e.g. Battaglia & Aki 2003; Kumagai *et al.* 2010; Ogiso *et al.* 2015), we used $Q = 60$ as a typical value at our studied volcanoes. To estimate A_s and I_s, we assumed that the seismic sources during the eruptions were at the summit craters of the individual volcanoes (Fig. 3), and no grid search in space to estimate source locations in the ASL method was performed. We used a two-pole Butterworth filter with corner frequencies of 5 and 10 Hz in the Seismic Analysis Code (Goldstein *et al.* 2003) and $f = 7.5$ Hz. To test the sensitivity of our analysis to our parameter selection, we varied the values of Q and β, and found that the estimates of A_s were more sensitive to decreasing Q and β. For 20 per cent decreases and increases in Q and β, respectively, at Kirishima, A_s increased and decreased by roughly 20–25 and 10–15 per cent, respectively. These A_s variations are within the standard deviations of our estimates of A_s at different stations, indicating that the effects of Q and β may not be large.

2.2 Seismic and plume height data

We used vertical seismograms from local networks of the Japan Meteorological Agency (JMA) at Sakurajima, Kuchinoerabujima, Ontake and Kirishima; the Earthquake Research Institute (ERI); The University of Tokyo and the National Research Institute for Earth Science and Disaster Resilience (NIED) at Kirishima; and the Institute Geofísico, Escuela Politécnica Nacional of Ecuador (IG-EPN) at Tungurahua (Kumagai *et al.* 2007, 2010; Fig. 3). These andesitic volcanoes produce sub-Plinian, Vulcanian, phreato-magmatic and phreatic eruptions (see the Appendix). All stations used in this study were 1–10 km from the individual craters (Fig. 3). Plume height data measured from the craters of the individual volcanoes were adopted from Steffke *et al.* (2010), Shimbori *et al.* (2013), Kozono *et al.* (2014), and JMA and IG-EPN reports (Table 1). No corrections for site amplification were performed in this study. We note, however, that estimates of A_s and I_s using borehole seismic data were clearly smaller than those using surface station data (Fig. 4), indicating that station site conditions affected our estimates of A_s and I_s. Therefore, we excluded borehole station data and used only surface station data to homogenize station site conditions, and our estimates as the averages of surface station data are easily comparable to those at seismic networks at other volcanoes, where surface stations are commonly deployed. This procedure follows that used by Kumagai *et al.* (2013) to compare the source amplitude with seismic magnitude for various volcano-seismic events at different volcanoes.

Seismic data from surface stations can be more easily affected by air–ground coupling than data from borehole stations (Ichihara *et al.* 2012; Matoza & Fee 2014). Seismic waves generated by infrasonic waves were clearly identified for explosion events at Tungurahua; for those events, we used time windows preceding the arrivals of the infrasonic waves to estimate A_s following Kumagai *et al.* (2013). Seismic waveforms of eruption tremor signals at Tungurahua were also affected by infrasonic waves. Kumagai *et al.* (2015) indicated that the ASLs of explosion events at Tungurahua estimated from seismic amplitudes contaminated by infrasonic waves were not near the summit; however, the ASLs of eruption tremor signals at Tungurahua were near the summit. These results suggest that the ASL method failed to correctly determine the source locations for seismic signals largely contaminated by infrasonic signals and that our analysed tremor signals located near the summit were dominantly radiated from their seismic sources at the summit crater. Ichihara (2016) showed that seismic data of eruption tremor signals during

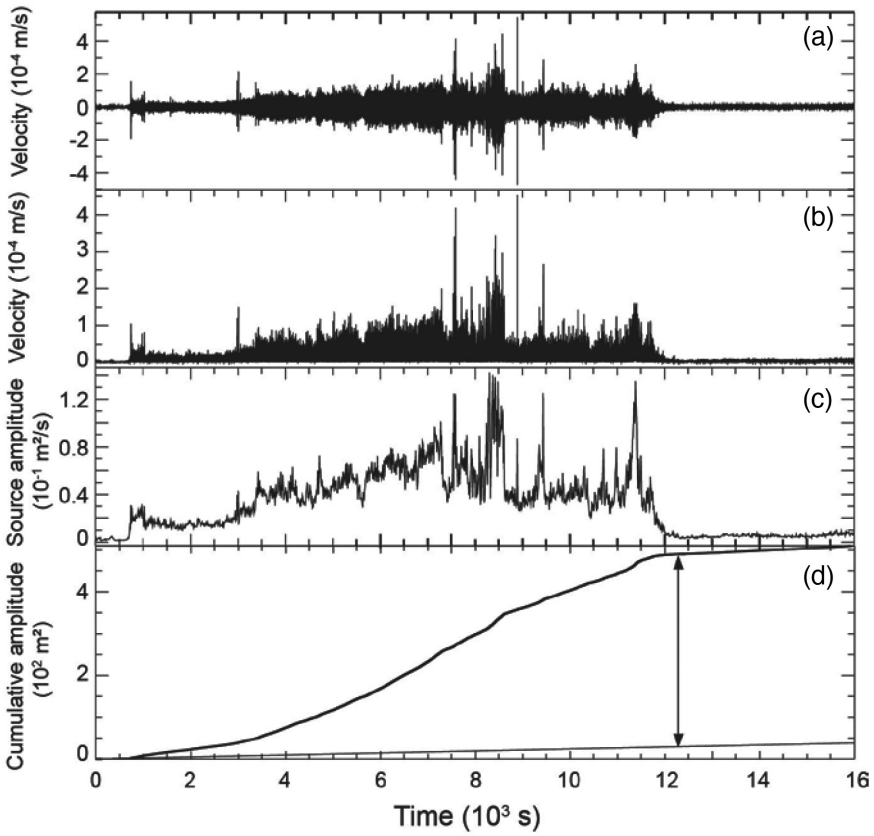

Figure 2. Estimation of cumulative source amplitude I_s. (a) Vertical velocity waveform in the 5–10 Hz band at station SMW during the first phase (Phase 1) of the 2011 Kirishima sub-Plinian eruptions. (b) Envelope of the waveform in (a). (c) Source amplitude function estimated from the envelope seismogram in (b) corrected for geometrical spreading and medium attenuation in individual 10-s time windows. (d) Time integration of the function in (c) (thick line) and the linear trend estimated from pre-tremor noise (thin line). The offset of the time-integrated function from the trend line (arrows) was taken as I_s.

the 2011 Kirishima eruptions in the 1–7 Hz band at station SMN, closest to the crater of Kirishima, were dominated by seismic energy than acoustic energy, and we confirmed this observation by our visual comparison of the seismic waveforms with the infrasonic waveforms in the 5–10 Hz band at this station. Using data from stations equipped with both seismic and infrasonic sensors at the other studied volcanoes, we visually confirmed that our analysed seismic waveforms were not largely contaminated by infrasound waves.

3 RESULTS

Our results highlight power-law relations between A_s and I_s for eruption tremors and explosion events (Fig. 5a). By comparing individual plume height estimates (H, km; Table 1) with A_s for eruption tremors and explosion events, we found that H is described by a power-law relation with A_s (Fig. 5b) for eruption tremors,

$$H = 11.3 A_s^{0.25}, \tag{10}$$

and for explosion events,

$$H = 7.80 A_s{}^{0.34}. \tag{11}$$

We note large scatter in our results for explosion events. H is also described by power-law relations with I_s for both eruption tremors and explosion events; our estimated power-law relations among A_s, I_s and H for eruption tremors and explosion events with errors on the coefficients and power-law indices are listed in Table 2.

The relation for eruption tremor (eq. 10) is based on the maximum seismic amplitudes and associated maximum plume heights during individual eruptive episodes. However, these data alone are insufficient to fully characterize their relation. More detailed comparison between H and A_s is possible for sub-Plinian eruptions at Kirishima in 2011 by using plume heights from continuously recorded weather radar data with time intervals of 10 min (Shimbori *et al.* 2013; Kozono *et al.* 2014; Fig. 6). We estimated A_s in each 10-min time window from seismograms recorded during eruptions P1–P3 and compared those values with the corresponding plume heights (Fig. 6a). Moreover, we compared those values with the relation between the maximum H and A_s values for sub-Plinian eruptions at Tungurahua and Kirishima (Fig. 7a). To derive the relation between H and A_s for Kirishima, we assumed the following exponential function:

$$H = \alpha \left[1 - \mathrm{e}^{\frac{-(A_s - \delta)}{\gamma}}\right] \quad (\delta \le A_s \le 0.1), \tag{12}$$

and $H = 0$ for $A_s < \delta$. Here, α, γ and δ are fitting parameters. We performed a grid search to find their best-fit values. The highest plumes (6–7 km) are explained by eq. (10), whereas plumes with $H < 6$ km deviate from this relation (Fig. 7a) and are better explained by A_s data for eruption tremors:

$$H = \begin{cases} 0 & (A_s < 0.003) \\ 6.97\left[1 - \exp\left\{-\frac{(A_s - 0.003)}{0.02}\right\}\right] & (0.003 \le A_s \le 0.15) \end{cases} \tag{13}$$

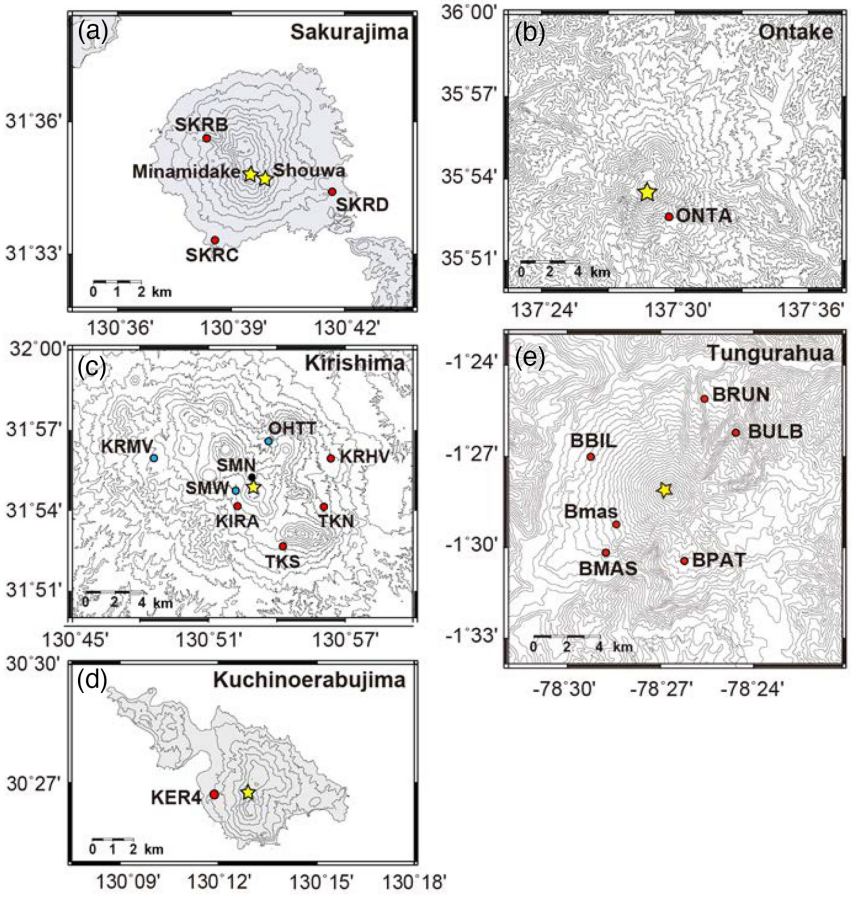

Figure 3. Seismic stations used in this study at (a) Sakurajima, (b) Ontake, (c) Kirishima, (d) Kuchinoerabujima and (e) Tungurahua. We did not use data from stations within 1 km of the craters, as they may not satisfy the assumption of isotropic radiation of *S* waves used in our seismic data analysis. Stations shown by blue circles at Kirishima were used to derive the estimates of A_s with 10-min intervals shown in Figs 6–11. These stations provided good quality continuous data without gaps during the P1–P3 eruptions. Data from these and other stations except for SMN at Kirishima were used to derive the maximum A_s values during the individual P1–P3 eruptions in Fig. 5.

and

$$H = 11.3{A_s}^{0.25} \quad (A_s > 0.15). \tag{14}$$

Here, we estimated $A_s = 0.15$ m^2 s^{-1} as the value at the intersection of the exponential and power-law relations near $H = 6$ km in Fig. 7(a). Fig. 7(b) shows that plume height estimates based on eqs (13) and (14) better reproduced the fluctuations of the observed time-series plume height data at Kirishima compared to estimates using the single power-law relation of eq. (10).

During the 2011 Kirishima eruptions, Kozono *et al.* (2014) estimated eruption volume flux ($\dot{V}$, m^3 s^{-1}) from tiltmeter data (Ueda *et al.* 2013). Comparison to our estimates of A_s (Fig. 8) indicates the following relation when $A_s < 0.1$ m^2 s^{-1}:

$$\dot{V} = 3970A_s. \tag{15}$$

In previous studies, the relation among seismic amplitudes, plume heights and eruption volume flux has been also investigated using reduced displacement D_R (cm^2). D_R has been related to plume height as (McNutt 1994)

$$H = 1.11{D_R}^{0.556}, \tag{16}$$

and to vent area (McNutt & Nishimura 2008). Tremor during the waxing phase of the 2016 eruption of Pavlof volcano, Alaska, followed the relation of eq. (16) (Fee *et al.* 2017; Haney *et al.* 2018). Ichihara (2016) suggested that eq. (16) is consistent with a linear relationship between the powers of eruption tremors ($D_R{}^2$) and $\dot{V}$ during the 2011 Kirishima eruptions. Although D_R is conceptually similar to A_s, no frequency band is specified and the peak-to-peak amplitude is used to estimate D_R. To investigate the relation between A_s and D_R, we compared D_R with A_s and H for eruption tremors at Kirishima and individual explosion events and eruption tremors at Tungurahua. D_R was estimated by the following equation using vertical seismograms with a 1-Hz high-pass filter:

$$D_R = \frac{1}{N}\sum_{i=1}^{N} a_i r_i/(2\sqrt{2}), \tag{17}$$

where a_i is the peak-to-peak amplitude given in displacement (cm) and r_i is the source-station distance (cm) at the ith station. Our comparison indicates that D_R is correlated with A_s (Fig. 9), but our estimates of D_R are not consistent with eq. (16) (Fig. 10). We also note that the data of smaller eruptions (H less than 2–3 km) at various volcanoes including Krishima are deviated from the relation of eq. (16) (Fig. 10) as pointed out by Johnson *et al.* (2005).

Table 1. Eruptive episodes and estimates of source amplitudes (A_s) and cumulative source amplitudes (I_s). The plume height (H) above the crater in each eruption episode was adopted from the numbered references listed in the footnote. Eruption dates and times at Tungurahua are Coordinated Universal Time (UTC), and other eruption dates are Japan Standard Time (UTC + 9 h).

Volcano	Date	Event type	A_s ($m^2\ s^{-1}$)	I_s (m^2)	H (km)	Reference
Sakurajima	2013.8.18 16:31	Explosion	7.95×10^{-2}	9.45	5.0	1
	2015.9.28 7:34	Explosion	4.38×10^{-2}	8.20×10^{-1}	1.3	2
	2015.9.28 4:59	Explosion	1.74×10^{-2}	2.19×10^{-1}	1.1	3
	2015.9.27 23:51	Explosion	1.19×10^{-2}	5.27×10^{-1}	1.3	4
	2015.9.27 17:53	Explosion	6.24×10^{-2}	8.47×10^{-1}	1.6	5
	2015.9.27 15:18	Explosion	3.06×10^{-2}	3.57×10^{-1}	Unknown	
	2015.9.26 23:56	Explosion	5.97×10^{-2}	9.70×10^{-1}	Unknown	
	2015.9.26 21:37	Explosion	3.00×10^{-2}	4.62×10^{-1}	1.3	6
	2015.9.26 20:14	Explosion	1.53×10^{-2}	4.72×10^{-1}	1.2	7
	2015.9.12 4:20	Explosion	7.37×10^{-3}	7.41×10^{-2}	1.5	8
	2015.9.12 3:49	Explosion	1.35×10^{-2}	2.36×10^{-1}	1.4	9
	2015.9.12 1:36	Explosion	4.59×10^{-3}	4.91×10^{-1}	1.1	10
	2015.9.12 0:16	Explosion	8.01×10^{-3}	6.36×10^{-1}	1.3	11
	2015.9.11 20:41	Explosion	4.81×10^{-3}	1.39×10^{-1}	1.0	12
	2015.1.23 20:36	Explosion	7.68×10^{-2}	3.34	4.0	13
	2015.2.21 0:53	Explosion	1.01×10^{-1}	3.11	3.5	14
	2015.3.17 6:33	Explosion	5.64×10^{-2}	3.31	3.3	15
	2015.4.24.9:16	Explosion	2.78×10^{-2}	12.2	4.0	16
	2015.5.21 10:20	Explosion	5.72×10^{-2}	3.88	4.3	17
	2015.6.1 12:33	Explosion	1.73×10^{-2}	2.04	3.3	18
Kuchinoerabujima	2015.5.29 9:59	Explosion	4.17×10^{-1}	18.9	9.0	19
Ontake	2014.9.27 11:52	Tremor	2.05×10^{-1}	1.92×10^{2}	7.0	20
Kirishima	Phase1 (P1)[a]	Tremor	1.26×10^{-1}	3.43×10^{2}	7.08	21, 22
	Phase2 (P2)[b]	Tremor	1.07×10^{-1}	4.13×10^{2}	6.98	21, 22
	Phase3 (P3)[c]	Tremor	1.19×10^{-1}	1.49×10^{2}	6.98	21, 22
	2011.1.26 14:49	Explosion	1.86×10^{-1}	40.1	1.98	21, 22
	2011.1.27 15:41	Explosion	1.85×10^{-1}	8.26	6.38	21, 22
	2011.1.28 12:47	Explosion	3.61×10^{-1}	8.52	3.58	21, 22
	2011.1.29 6:40	Explosion	1.48×10^{-2}	15.9	3.18	21, 22
	2011.2.1 23:34	Explosion	2.04×10^{-2}	1.23	5.78	21, 22
	2011.2.2 5:25	Explosion	2.49×10^{-1}	4.63	5.08	21, 22
	2011.2.2 10:47	Explosion	1.15×10^{-1}	3.50	3.78	21, 22
	2011.2.2 19:17	Explosion	2.12×10^{-1}	3.52	2.98	21, 22
	2011.2.2 22:02	Explosion	7.01×10^{-2}	2.51	5.78	21, 22
Tungurahua	2006.7.14 21:00–7.15 7:59	Tremor	8.29×10^{-1}	3.70×10^{3}	9.4	23
	2006.8.17 0:00–7:59	Tremor	1.07	4.62×10^{3}	15.4	23
	2010.5.28 13:46–21:39	Tremor	5.30×10^{-1}	3.71×10^{3}	10	24
	2012.12.16 12:34–21:55	Tremor	3.45×10^{-1}	1.84×10^{3}	7.2	25
	2013.7.14 11:46–12:51	Tremor	2.81×10^{-1}	5.60×10^{2}	8.3	26
	2014.2.1 22:38–2.2 3:35	Tremor	5.76×10^{-1}	2.05×10^{3}	8.7	27

[a]2011.1.26 15:27–18:41. [b]2011.1.26 21:34–27 4:57. [c]2011.1.27 16:20–17:48.
[1]JMA (2013); [2]JMA (2015a); [3]JMA (2015b); [4]JMA (2015c); [5]JMA (2015d); [6]JMA (2015e); [7]JMA (2015f); [8]JMA (2015g); [9]JMA (2015h); [10]JMA (2015i); [11]JMA (2015j); [12]JMA (2015k); [13]JMA (2015l); [14]JMA (2015m); [15]JMA (2015n); [16]JMA (2015o); [17]JMA (2015p); [18]JMA (2015q); [19]JMA (2015r); [20]JMA (2014); [21]Shimbori *et al.* (2013); [22]Kozono *et al.* (2014); [23]Steffke *et al.* (2010); [24]IG-EPN (2010); [25]IG-EPN (2012); [26]Washington VAAC (2013); [27]IG-EPN (2014).

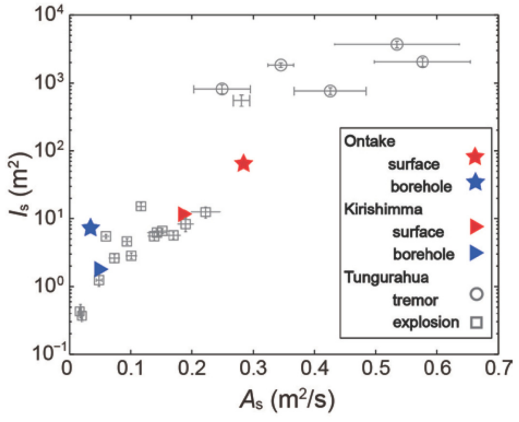

Figure 4. Comparison of surface and borehole station data. I_s and A_s data from surface and borehole stations at Ontake and Kirishima are compared with surface station data at Tungurahua.

4 DISCUSSION

Our estimated linear relation between A_s and $\dot{V}$ for the 2011 Kirishima eruptions (eq. 15) is different from the proportionality between seismic power and $\dot{V}$ reported by Ichihara (2016). We examined this difference based on characteristics of scattered wavefields, which depend on frequency and source-station distance. We found that $\dot{V}$ proportional to A_s when we use seismic data from stations SMW, OHTT and KRMV, which are located more than 1 km from the crater (Fig. 11c, eq. 15). However, $\dot{V}$ and A_s are not proportional when we use only data at station SMN, located at 800 m from the crater (Fig. 11d). We also compared D_R with $\dot{V}$ (Figs 11a and b). A proportionality between $\dot{V}$ and $D_R{}^2$ roughly holds at station SMN (Fig. 11b), as suggested by Ichihara (2016). However, when we use data at stations SMW, OHTT and KRMV, the relation between D_R and $\dot{V}$ deviates from this proportionality (Fig. 11a). Assuming an S-wave velocity of 1400 m s^{-1}, the wavelength of an S wave in the 5–10 Hz frequency band is about 140–280 m. The scattering mean free path for S waves is estimated to be around 500 m at volcanoes (e.g. Wegler 2003; Yamamoto & Sato 2010). Therefore, the wavefields at stations SMW, OHTT and KRMV are regarded as far-field and multiple scattering dominates, resulting in isotropic radiation of S waves. In this case, estimates of A_s may be simply related to the moment rate function ($\dot{M}$) or $\dot{V}$ for a moment tensor source model as explained below. At station SMN, however, single scattering dominates and isotropic radiation of S waves may not hold. In this case, estimates of A_s are affected by source mechanisms and a simple proportional relation between A_s and $\dot{V}$ may not exist. Thus, the proportionality between A_s and $\dot{V}$ holds only for seismic data in

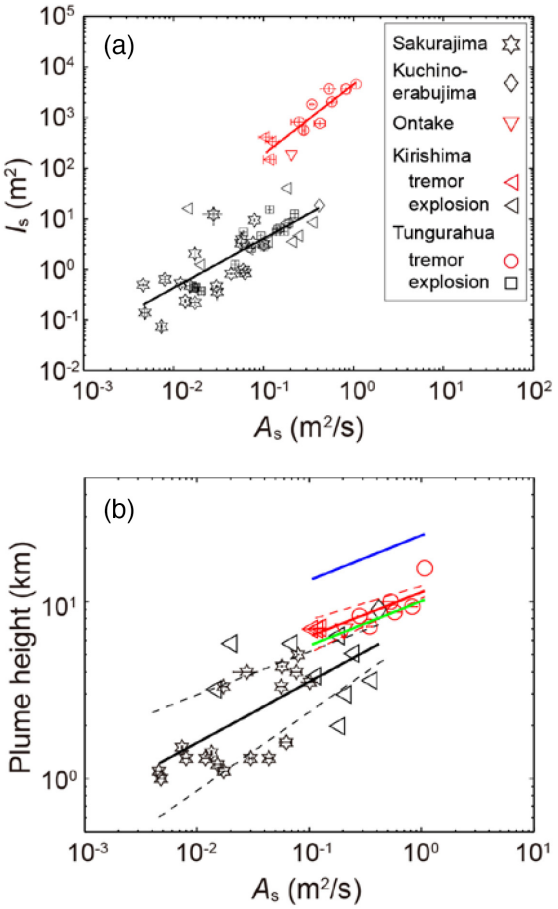

Figure 5. Power-law relations between the source amplitude (A_s) and (a) cumulative source amplitude (I_s) and (b) plume height. The relations shown by red and black lines in (a) and (b) were derived from the least-squares linear fits on the log–log plots. Horizontal and vertical error bars show probable errors of the estimates based on individual station data. (a) A_s plotted against I_s for eruption tremors (red symbols) and explosion events (black symbols). Red and black lines represent the best-fit power-law relations between A_s and I_s for eruption tremors and explosion events, respectively. (b) Plume heights plotted as a function of A_s. Symbols and colours as in (a). Red and black lines represent the best-fit power-law relations between A_s and plume height for eruption tremors and explosion events, respectively. Dashed lines show the error ranges of the best-fit power-law relations estimated for eruption tremors and explosion events. Blue and green lines represent plume heights estimated by using eq. (31) with $u = 0$ and 80 m s^{-1}, respectively.

Table 2. Power-law relations among source amplitude A_s (m^2 s^{-1}), cumulative source amplitude I_s (m^2) and plume height H (km above the crater) for eruption tremors and explosion events. Standard errors of the coefficients and power-law indices (e.g. Larsen & Marx 2012) are shown.

Eruption tremor	$I_s = (46 \pm 12) \times 10^2 A_s{}^{1.39\pm0.21}$
	$H = (11.3 \pm 0.92) A_s{}^{0.25\pm0.06}$
	$H = (3.10 \pm 0.95) I_s{}^{0.15\pm0.04}$
Explosion events	$I_s = (38 \pm 15) A_s{}^{0.98\pm0.12}$
	$H = (7.8 \pm 1.8) A_s{}^{0.34\pm0.07}$
	$H = (2.10 \pm 0.19) I_s{}^{0.30\pm0.05}$

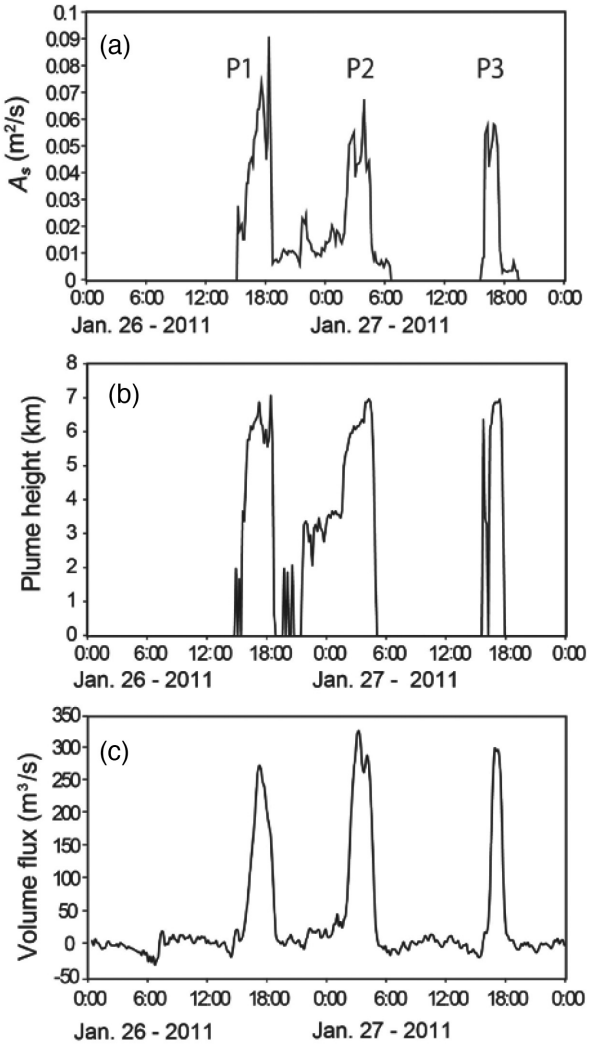

Figure 6. Time-series data of (a) A_s, (b) H and (c) eruption volume flux ($\dot{V}$) during the P1–P3 eruptions at Kirishima (times are Japan Standard Time). Plume height data were continuously recorded by weather radars at 10-min time intervals (Shimbori *et al.* 2013; Kozono *et al.* 2014) and $\dot{V}$ was estimated from tiltmeter data (Kozono *et al.* 2014).

the 5–10 Hz frequency band and at source-station distances > 1 km. Such a difference in the wavefields may also affect D_R estimates. The peak amplitudes used to estimate D_R contain low-frequency components and are affected by the source mechanism and source time function, which may cause scatter in the D_R estimates as shown in Fig. 10.

We consider the proportionality relation between A_s and $\dot{V}$ based on the equivalent source theory of Haney *et al.* (2018). We assume that the seismic source of eruption tremor is a vertical crack or cylindrical conduit and that the plume is a jet flow exiting the conduit. In the case of a crack source, the source volume (V_s) is expressed as

$$V_s = WLd, \tag{18}$$

where W, L and d are crack width, length and aperture, respectively. Under the assumption that the crack volume changes with $L \propto d$, the change in the source volume per unit time $\dot{V}_s$ in angular frequency ω is expressed as

$$\dot{V}_s \propto \omega d^2 W. \tag{19}$$

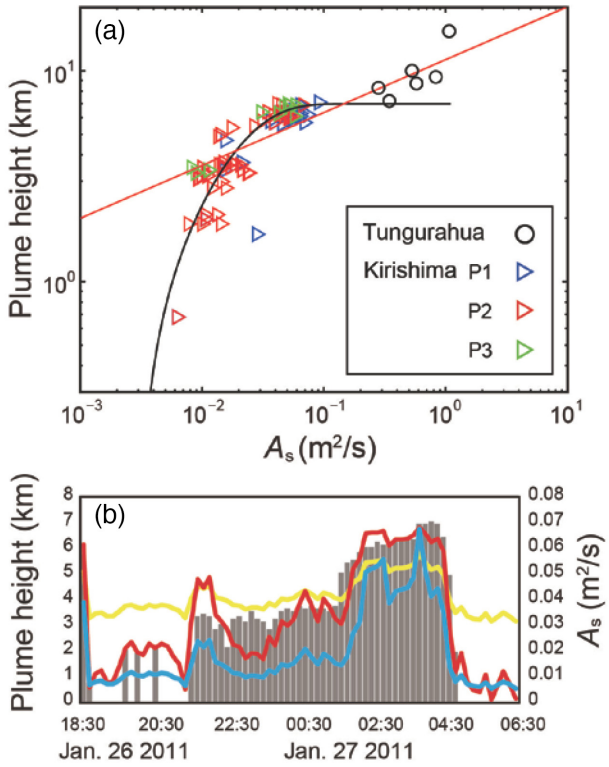

Figure 7. Plume height estimates based on the source amplitude. (a) Observed plume heights (H) plotted against the source amplitudes (A_s) of eruption tremors at Kirishima and Tungurahua. For sub-Plinian eruptions P1–P3 at Kirishima, plume heights were continuously recorded by weather radars at time intervals of 10 min (Shimbori *et al.* 2013; Kozono *et al.* 2014), and we estimated A_s in each corresponding interval. Red and black lines are plume height predictions given by eqs (10) and (13), respectively. (b) Time-series plume height estimates using A_s during the P2 eruption at Kirishima (times are Japan Standard Time). Grey bars and the blue line show observed H and A_s, respectively. Yellow and red lines represent H as estimated by eqs (10), (13) and (14), respectively.

Here, to consider the relation between tremor frequencies and source volume changes, we use the Strouhal number (S_t) expressed as

$$S_t = \frac{\omega d}{v_e}, \tag{20}$$

where v_e is the exit velocity of the jet flow from the crack (Haney *et al.* 2018). S_t can be considered constant over a wide range of flow conditions (Woulff & McGetchin 1976), so we can assume $\omega d \propto v_e$. Therefore, eq. (19) can be expressed as

$$\dot{V}_s \propto dW v_e = \dot{V}. \tag{21}$$

For a cylindrical conduit as the seismic source, V_s is expressed as

$$V_s = \pi {R_c}^2 L_c, \tag{22}$$

where R_c and L_c are conduit radius and length, respectively. Under the assumption that the source volume changes with $R_c \propto L_c$, $\dot{V}_s$ is expressed using ω as

$$\dot{V}_s \propto \pi \omega {R_c}^3. \tag{23}$$

In this case, $\omega R_c \propto v_e$ holds when S_t is constant. Therefore, eq. (23) can be expressed as

$$\dot{V}_s \propto \pi {R_c}^2 v_e = \dot{V}. \tag{24}$$

For a moment tensor source model with the assumption of far-field S waves, S-wave velocity amplitude (v) can be expressed using A_s and the moment rate function ($\dot{M}$) as

$$v \propto \frac{A_s}{r} e^{-\frac{\pi f}{Q\beta} r} \propto \frac{\omega \dot{M}}{\rho \beta^3 r} e^{-\frac{\pi f}{Q\beta} r}, \tag{25}$$

where ρ, β, r, f and Q are density, S-wave velocity, source-station distance, frequency and medium attenuation, respectively (e.g. Aki & Richards 2002). Therefore, we obtain the following relation:

$$\dot{M} \propto \frac{\rho \beta^3}{\omega} A_s. \tag{26}$$

Using $\dot{M} = \mu \dot{V}_s$ and eq. (26), where μ is rigidity (e.g. Aki & Richards 2002), we can derive the proportionality between A_s and $\dot{V}_s$. In turn, from eqs (21) and (24), we obtain the proportionality between A_s and $\dot{V}$.

Plumes that reach the upper troposphere and stratosphere rise buoyantly because of air entrainment (Morton *et al.* 1956; Settle 1978; Sparks 1986), which is theoretically described by $H \propto \dot{V}^{1/4}$ for Plinian eruptions. The following empirical relation fits data from Plinian eruptions at various volcanoes (Mastin *et al.* 2009):

$$H = 2.00 \dot{V}^{0.241}. \tag{27}$$

The power-law relation for eruption tremors (eq. 14) is similar to these theoretical and empirical relations, suggesting that A_s may be proportional to $\dot{V}$. Combining eqs (14) and (27), we obtain the following relation when $A_s > 0.15$ m^2 s^{-1}:

$$\dot{V} = 1316 A_s. \tag{28}$$

We also estimated the linear relation between A_s and $\dot{V}$ from the observation data at Kirishima when $A_s < 0.1$ m^2 s^{-1} (eq. 15). Thus, these results suggest that the proportionality between A_s and $\dot{V}$ holds over a wide range of A_s values, although the proportionality coefficients in eqs (15) and (28) are different. Mastin *et al.* (2009) mainly studied large eruptions with $H > 10$ km, which were not extensively examined in this study, and the coefficient would be different for such large eruptions.

Eruption plumes comprise a lower, momentum-driven gas jet and an upper, buoyant convective plume (Wilson 1976; Woods 1988). Plume height is thus affected by the vent radius, initial velocity, initial temperature and initial mass fraction of gas (Woods 1988; Suzuki *et al.* 2005). The difference between the relations for plumes reaching the lower troposphere (eq. 13) and upper troposphere and stratosphere (eq. 14) may be associated with these source parameters. When initial velocity and initial temperature are high, vent radius is large (but not extremely large) and the initial gas mass fraction is small, plumes can stably rise to the upper troposphere and stratosphere (Woods 1988). For such plumes, a 1/4 power-law relation between H and $\dot{V}$ holds such as eq. (27). In this case, H is given in terms of A_s by eq. (14) based on the proportionality between $\dot{V}$ and A_s. Deviations from the power-law relation (Fig. 7a and eq. 13) may occur when these conditions are not satisfied. Eq. (13) indicates that a plume will not rise if A_s is less than 3.0×10^{-3} m^2 s^{-1}, corresponding to a mass flux of about 3×10^4 kg s^{-1} dense-rock equivalent. Indeed, Plinian eruptions with eruptive mass flux less than 3×10^4 kg s^{-1} are rarely reported (Mastin *et al.* 2009). We note that if source conditions are extremely different from those of the eruptions analysed herein, our proposed relations between H and A_s may not hold.

The eruption mass flux q (kg s^{-1}) during the 2011 Kirishima eruptions is given as (Kozono *et al.* 2014)

$$q = 2.5 \dot{V} \rho, \tag{29}$$

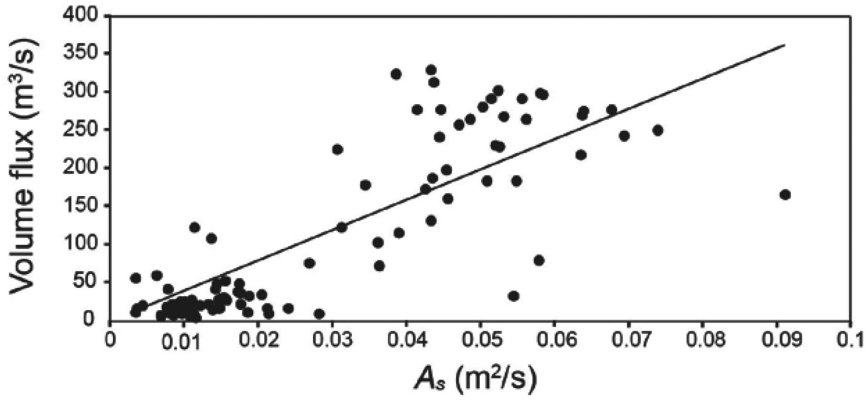

Figure 8. Correlation of eruption volume flux estimated from tiltmeter data during the P1–P3 eruptions at Kirishima (Kozono *et al.* 2014) with source amplitude A_s estimated in the corresponding 10-min time intervals. The solid line represents the linear relation of eq. (15) derived from the least-squares fits with a correlation coefficient of 0.69.

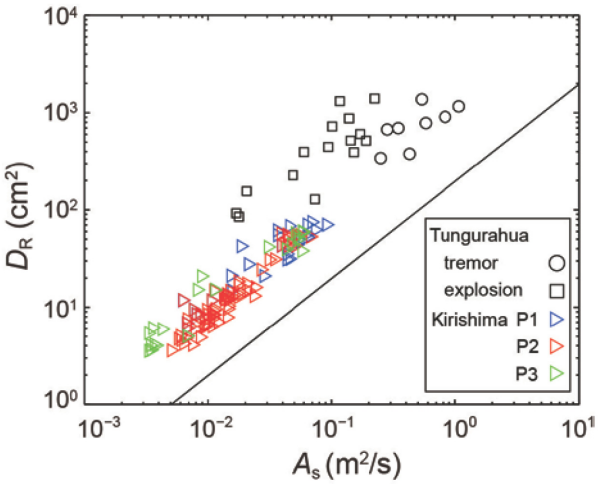

Figure 9. Reduced displacement (D_R) and source amplitude (A_s) of selected eruptions. D_R plotted against A_s for eruption tremors at Kirishima (D_R values for the P1–P3 eruptions were estimated for the corresponding 10-min time windows used to estimate A_s) and explosion events and eruption tremors at Tungurahua. The black line represents a line with the slope of 1 ($D_R \propto A_s$) for reference.

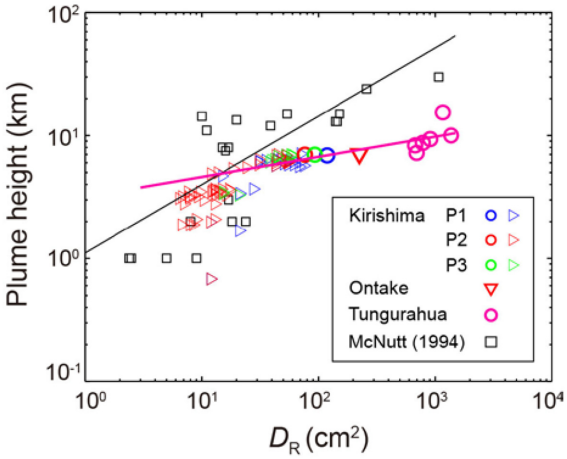

Figure 10. Eruption plume heights as a function of reduced displacement D_R. Maximum plume heights are compared to D_R for eruption tremors during the individual eruptions at Kirishima (P1–P3 eruptions shown by blue, red and green circles, respectively), Tungurahua (magenta circles) and Ontake (red inverted triangle). D_R values at Kirishima estimated in 10-min time windows for the P1–P3 eruptions (blue, red and green sideways triangles, respectively) are also shown. The relation between D_R and plume height (magenta line) derived from the least-squares fits on the log–log plots of the data for the maximum plume heights at Kirishima and Tungurahua (circles) is shown. For comparison, black squares show the data at various volcanoes from table 2 of McNutt (1994), and their relation given by eq. (16) is plotted (black line).

where $\rho = 2500$ kg m^{-3} is the density of dense rock and 2.5 is a correction factor for magma compressibility. Woodhouse *et al.* (2013) derived the following model relationship between plume height and eruption mass flux accounting for the effects of wind:

$$H = 0.318 q^{0.253} \frac{1 + 1.373\tilde{W}}{1 + 4.266\tilde{W} + 0.3527\tilde{W}^2}, \tag{30}$$

where $\tilde{W} = 1.44u/(NH_1)$ and N is a buoyancy frequency of 0.0108 s^{-1} and u is wind velocity at a reference altitude of $H_1 = 11$ km. Combining eqs (15) and (29) and using the model relationship of eq. (30), we obtain

$$H = 23.61 A_s^{0.253} \frac{1 + 0.0166u}{1 + 0.0517u + 5.182 \times 10^{-5}u^2}. \tag{31}$$

During the 2011 Kirishima eruptions, a maximum wind velocity of 80 m s^{-1} was estimated at 11 km above sea level (Hashimoto *et al.* 2012). Plume height estimates as a function of A_s using eq. (31) with $u = 80$ m s^{-1} are consistent with the Kirishima data and similar to those obtained using eq. (10) (Fig. 5b). The relation derived by combining eq. (28) for $A_s > 0.15$ m^2 s^{-1} and eq. (29) and using eq. (30) with $u = 80$ m s^{-1} is similar to eq. (31) when $u = 0$ m s^{-1}, which is not consistent with the Kirishima data (Fig. 5b). This result suggests that eq. (31) derived by using eq. (15) for $A_s < 0.1$ m^2 s^{-1} may be appropriate to estimate the height of plumes reaching the upper troposphere and lower stratosphere, though further studies are required for larger eruptions producing plumes that reach the upper stratosphere. We note that the error in plume height estimates is about 2–3 km when $A_s = 0.01$–0.1 m^2 s^{-1} (Fig. 5b, Table 2), which should be considered when estimating plume heights from A_s.

5 CONCLUDING REMARKS

The source amplitude A_s can be estimated in seconds without any complicated data processing after seismic data acquisition, whereas

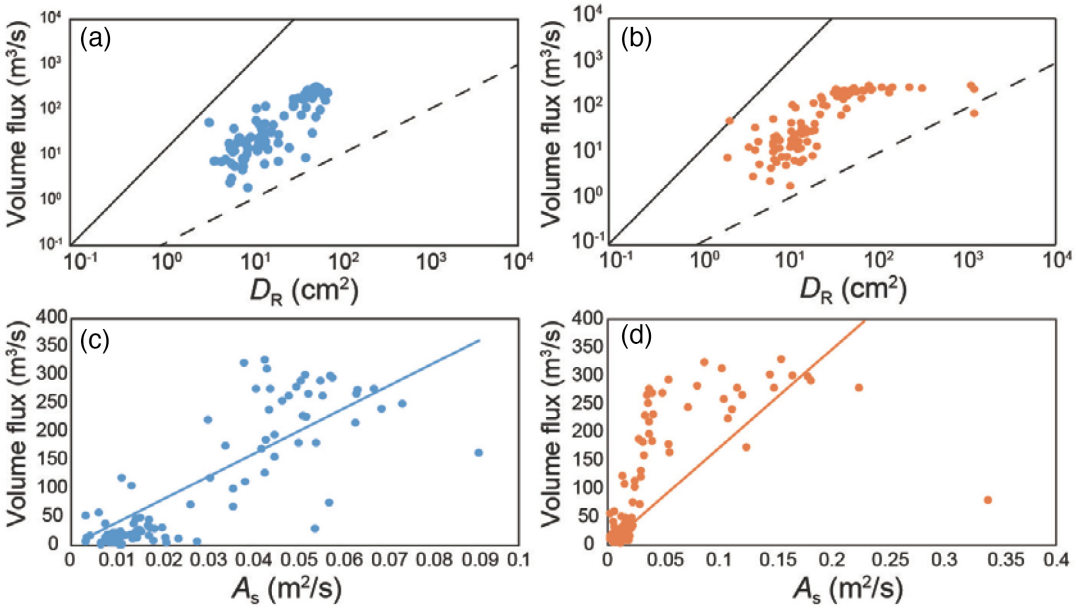

Figure 11. Relations between volume flux ($\dot{V}$) and (a and b) reduced displacement (D_R) and (c and d) source amplitude (A_s) for the 2011 Kirishima eruptions (P1–P3). D_R and A_s values for the P1–P3 eruptions were estimated during 10-min time windows. Blue (a and c) and orange (b and d) dots indicate our estimates using data from three stations farther than 1 km from the crater (OHTT, SMW and KRMV) and station SMN only within 1 km of the crater, respectively (Fig. 3). Solid and dashed lines in (a) and (b) represent lines with the slopes of 2 ($\dot{V} \propto D_R^2$) and 1 ($\dot{V} \propto D_R$), respectively, for reference. The blue line in (c) is given by eq. (15), and the orange line in (d) is our linear fit to the data. Note that the scales are logarithmic in (a and b) and linear in (c and d).

eruption plumes take minutes to reach their maximum heights. Thus, it may be possible to predict plume heights using A_s based on eqs (13) and (14) or eq. (31) for Plinian eruptions and eq. (11) for Vulcanian eruptions. The effects of wind must be considered for real-time application in which assumed or predicted wind velocities may be used in eq. (31). The universality of the scaling relations between A_s and H at other volcanoes and the precision of real-time plume height estimates at our studied volcanoes should be investigated in future studies. Because seismic networks are commonly used to monitor active volcanoes, the approach proposed herein can be easily applied. Our study also demonstrates that A_s is related to eruption volume flux, and thus detailed information about temporal variations in eruption volume flux may be obtained from A_s. During the 2011 Kirishima eruptions, C-band (∼5 cm wavelength) weather radar was used to observe plume heights (Shimbori *et al.* 2013), limiting the spatial and temporal resolutions of available plume height data. Recently, X-band (∼3 cm wavelength) multiparameter radar has been used to observe eruption plumes with high spatial and temporal resolutions (e.g. Marzono *et al.* 2006; Maki *et al.* 2016). A combined approach using A_s and such high-resolution plume images would contribute to a better understanding of eruptive processes.

ACKNOWLEDGEMENTS

We thank Tomofumi Kozono for sharing their eruption plume height data for the 2011 Kirishima eruptions and for useful discussions. We are also grateful to Patricia Mothes for useful comments about Tungurahua eruptions. Seismic data at Sakurajima, Kuchinoerabujima, Ontake and Kirishima were observed by the Japan Meteorological Agency (JMA) and provided through the National Research Institute for Earth Science and Disaster Resilience (NIED, http://www.vnet.bosai.go.jp/). Seismic data at Kirishima were observed by the Earthquake Research Institute (ERI), The University of Tokyo, and were provided through collaborative research managed by Mie Ichihara. Plume height data and their references are listed in Table 1. Comments from Robin Matoza and anonymous reviewers helped to improve the manuscript. This work was partly supported by JST/JICA SATREPS and the Integrated Program for Next Generation Volcano Research and Human Resource Development sponsored by MEXT.

REFERENCES

Aki, K. & Koyanagi, R., 1981. Deep volcanic tremor and magma ascent mechanism under Kilauea, Hawaii, *J. geophys. Res.,* **86**(B8), 7095–7109.

Aki, K. & Richards, P.G., 2002. *Quantitative Seismology,* 2nd edn, University Science Books.

Battaglia, J. & Aki, K., 2003. Location of seismic events and eruptive fissures on the Piton de la Fournaise volcano using seismic amplitudes, *J. geophys. Res.,* **108**(B10), 2364.

Battaglia, J., Aki, K. & Staudacher, T., 2005. Location of tremor sources and estimation of lava output using tremor source amplitude on the Piton de la Fournaise volcano: 2. Estimation of lava output, *J. Volc. Geotherm. Res.,* **147,** 291–308.

Battaglia, J., Got, J.-L. & Okubo, P., 2003. Location of long-period events below Kilauea Volcano using seismic amplitudes and accurate relative relocation, *J. geophys. Res.,* **108**(B12), 2553.

Bernard, B., Battaglia, J., Proaño, A., Hidalgo, S., Vasconez, F., Hernadez, S. & Ruiz, M., 2016. Relationship between volcanic ash fallouts and seismic tremor: quantitative assessment of the 2015 eruptive period at Cotopaxi volcano, Ecuador, *Bull. Volcanol.,* **78,** 80.

Chouet, B.A. & Matoza, R., 2013. A multi-decadal view of seismic methods for detecting precursors of magma movement and eruption, *J. Volc. Geotherm. Res.,* **252,** 108–175.

Institute Geofísico, Escuela Politécnica Nacional de Ecuador (IGEPN), 2010. Boletín especial del volcán Tungurahua No.9 (May, 2010), http://www.igepn.edu.ec/tungurahua-informes/tung-especiales/tung-e-2010/8877-informe-especial-tungurahua-no-9–1/file.

Institute Geofísico, Escuela Politécnica Nacional of Ecuador (IG-EPN), 2012. Informe Especial del Volcán Tungurahua No.9 (December, 2012), http://www.igepn.edu.ec/tungurahua-informes/tung-especiales/tung-e-2012/8866-informe-especial-no-9–16diciembre/file.

Institute Geofísico, Escuela Politécnica Nacional of Ecuador (IG-EPN), 2014. Informe Especial del Volcán Tungurahua No.3 (February, 2012), http://www.igepn.edu.ec/tungurahua-informes/tung-especiales/tung-e-2014/8899-informe-especial-tungurahua-no-3–3/file.

Fee, D., Haney, M.M., Matoza, R.S., Van Eaton, A.R., Cervelli, P., Schneider, D.J. & Iezzi, A.M., 2017. Volcanic tremor and plume height hysteresis from Pavlof Volcano, Alaska, *Science,* **355,** 45–48.

Goldstein, P., Dodge, D., Firpo, M. & Minner, L., 2003. SAC2000: Signal processing and analysis tools for seismologists and engineers, in *The IASPEI International Handbook of Earthquake and Engineering Seismology,* eds Lee, W.H.K. *et al.*, Academic Press.

Hall, M.L., Steele, A.L., Mothes, P.A. & Ruiz, M.C., 2013. Pyroclastic density currents (PDC) of the 16–17 August 2006 eruptions of Tungurahua volcano, Ecuador: geophysical registry and characteristics, *J. Volc. Geotherm. Res.,* **265,** 78–93.

Haney, M.M., Matoza, R.S., Fee, D. & Aldridge, D.F., 2018. Seismic equivalents of volcanic jet scaling laws and multipoles in acoustics, *Geophys. J. Int.,* **213,** 623–636.

Hashimoto, A., Shimbori, T. & Fukui, K., 2012. Tephra fall simulation for the eruptions at Mt. Shinmoe-dake during 26–27 January 2011 with JMANHM, *Sola,* **8,** 37–40.

Ichihara, M., 2016. Seismic and infrasonic eruption tremors and their relation to magma discharge rate: a case study for sub-Plinian events in the 2011 eruption of Shinmoe-dake, Japan, *J. geophys. Res.,* **121,** 7101–7118.

Ichihara, M., Takeo, M., Yokoo, A., Oikawa, J. & Ohminato, T., 2012. Monitoring volcanic activity using correlation patterns between infrasound and ground motion, *Geophys. Res. Lett.,* **39,** L04304.

Ichimura, M., Yokoo, A., Kagiyama, T., Yoshikawa, S. & Inoue, H., 2018. Temporal variation in source location of continuous tremors before ash–gas emissions in January 2014 at Aso volcano, Japan, *Earth Planets Space,* **70,** 125.

Japan Meteorological Agency (JMA), 2011. Monthly activity report of Kirishima (January, 2011), http://www.data.jma.go.jp/svd/vois/data/tokyo/STOCK/monthly_v-act_doc/fukuoka/11m01/505_11m01.pdf.

Japan Meteorological Agency (JMA), 2013. Monthly activity report of Sakurajima (August, 2013), http://www.data.jma.go.jp/svd/vois/data/tokyo/STOCK/monthly_v-act_doc/fukuoka/13m08/506_13m08.pdf.

Japan Meteorological Agency (JMA), 2014. Monthly activity report of Ontake (September, 2014), http://www.data.jma.go.jp/svd/vois/data/tokyo/STOCK/monthly_v-act_doc/tokyo/14m09/312_14m09.pdf.

Japan Meteorological Agency (JMA), 2015a. Observation report of eruption at Sakurajima (September, 28, 2015, 7:41), http://www.data.jma.go.jp/svd/vois/data/tokyo/STOCK/volinfo/VG20150928074101_506.html.

Japan Meteorological Agency (JMA), 2015b. Observation report of eruption at Sakurajima (September, 28, 2015, 5:06), http://www.data.jma.go.jp/svd/vois/data/tokyo/STOCK/volinfo/VG20150928050655_506.html.

Japan Meteorological Agency (JMA), 2015c. Observation report of eruption at Sakurajima (September, 28, 2015, 0:00), http://www.data.jma.go.jp/svd/vois/data/tokyo/STOCK/volinfo/VG20150928000048_506.html.

Japan Meteorological Agency (JMA), 2015d. Observation report of eruption at Sakurajima (September, 27, 2015, 18:03), http://www.data.jma.go.jp/svd/vois/data/tokyo/STOCK/volinfo/VG20150927180346_506.html.

Japan Meteorological Agency (JMA), 2015e. Observation report of eruption at Sakurajima (September, 26, 2015, 21:43), http://www.data.jma.go.jp/svd/vois/data/tokyo/STOCK/volinfo/VG20150926214334_506.html.

Japan Meteorological Agency (JMA), 2015f. Observation report of eruption at Sakurajima (September, 26, 2015, 20:21), http://www.data.jma.go.jp/svd/vois/data/tokyo/STOCK/volinfo/VG20150926202142_506.html.

Japan Meteorological Agency (JMA), 2015g. Observation report of eruption at Sakurajima (September, 12, 2015, 4:27), http://www.data.jma.go.jp/svd/vois/data/tokyo/STOCK/volinfo/VG20150912042705_506.html.

Japan Meteorological Agency (JMA), 2015h. Observation report of eruption at Sakurajima (September, 12, 2015, 3:55), http://www.data.jma.go.jp/svd/vois/data/tokyo/STOCK/volinfo/VG20150912035549_506.html.

Japan Meteorological Agency (JMA), 2015i. Observation report of eruption at Sakurajima (September, 12, 2015, 1:44), http://www.data.jma.go.jp/svd/vois/data/tokyo/STOCK/volinfo/VG20150912014431_506.html.

Japan Meteorological Agency (JMA), 2015j. Observation report of eruption at Sakurajima (September, 12, 2015, 0:23), http://www.data.jma.go.jp/svd/vois/data/tokyo/STOCK/volinfo/VG20150912002307_506.html.

Japan Meteorological Agency (JMA), 2015k. Observation report of eruption at Sakurajima (September, 11, 2015, 20:49), http://www.data.jma.go.jp/svd/vois/data/tokyo/STOCK/volinfo/VG20150911204947_506.html.

Japan Meteorological Agency (JMA), 2015l. Monthly activity report of Sakurajima (January, 2015), http://www.data.jma.go.jp/svd/vois/data/tokyo/STOCK/monthly_v-act_doc/fukuoka/15m01/506_15m01.pdf.

Japan Meteorological Agency (JMA), 2015m. Monthly activity report of Sakurajima (February, 2015), http://www.data.jma.go.jp/svd/vois/data/tokyo/STOCK/monthly_v-act_doc/fukuoka/15m02/506_15m02.pdf.

Japan Meteorological Agency (JMA), 2015n. Monthly activity report of Sakurajima (March, 2015), http://www.data.jma.go.jp/svd/vois/data/tokyo/STOCK/monthly_v-act_doc/fukuoka/15m03/506_15m03.pdf.

Japan Meteorological Agency (JMA), 2015o. Monthly activity report of Sakurajima (April, 2015), http://www.data.jma.go.jp/svd/vois/data/tokyo/STOCK/monthly_v-act_doc/fukuoka/15m04/506_15m04.pdf.

Japan Meteorological Agency (JMA), 2015p. Monthly activity report of Sakurajima (May, 2015), http://www.data.jma.go.jp/svd/vois/data/tokyo/STOCK/monthly_v-act_doc/fukuoka/15m05/506_15m05.pdf.

Japan Meteorological Agency (JMA), 2015q. Monthly activity report of Sakurajima (Jun, 2015), http://www.data.jma.go.jp/svd/vois/data/tokyo/STOCK/monthly_v-act_doc/fukuoka/15m06/506_15m06.pdf.

Japan Meteorological Agency (JMA), 2015r. Monthly activity report of Kuchinoerabujima (May, 2015), https://www.data.jma.go.jp/svd/vois/data/tokyo/STOCK/monthly_v-act_doc/fukuoka/15m05/509_15m05.pdf.

Japan Meteorological Agency (JMA), 2015s. Monthly activity report of Sakurajima (September, 2015), http://www.data.jma.go.jp/svd/vois/data/tokyo/STOCK/monthly_v-act_doc/fukuoka/15m09/506_15m09.pdf.

Johnson, J.B., Ruiz, M.C., Lees, J.M. & Ramon, P., 2005. Poor scaling between elastic energy release and eruption intensity at Tungurahua Volcano, Ecuador, *Geophys. Res. Lett.,* **32,** L15304.

Kozono, T., Ueda, H., Shimbori, T. & Fukui, K., 2014. Correlation between magma chamber deflation and eruption cloud height during the 2011 Shinmoe-dake eruptions, *Earth Planets Space,* **66,** 139.

Kumagai, H., Lacson, R., Jr, Maeda, Y., Figueroa, M.S., II & Yamashina, T., 2014. Shallow *S* wave attenuation and actively degassing magma beneath Taal Volcano, Philippines, *Geophys. Res. Lett.,* **41,** 6681–6688.

Kumagai, H., Mothes, P., Ruiz, M. & Maeda, Y., 2015. An approach to source characterization of tremor signals associated with eruptions and lahars, *Earth Planets Space,* **67,** 178.

Kumagai, H., Palacios, P., Ruiz, M., Yepes, H. & Kozono, H., 2011. Ascending seismic source during an explosive eruption at Tungurahua volcano, Ecuador, *Geophys. Res. Lett.,* **38,** L01306.

Kumagai, H. *et al.*, 2007. Enhancing volcano-monitoring capabilities in Ecuador, *EOS, Trans. Am. geophys. Un.,* **88,** 245–246.

Kumagai, H. *et al.*, 2010. Broadband seismic monitoring of active volcanoes using deterministic and stochastic approaches, *J. geophys. Res.,* **115,** B08303.

Kumagai, H. *et al.*, 2013. Source amplitudes of volcano-seismic signals determined by the amplitude source location method as a quantitative measure of event size, *J. Volc. Geotherm. Res.,* **257,** 57–71.

Kurokawa, A., Takeo, M. & Kurita, K., 2016. Two types of volcanic tremor changed with eruption style during 1986 Izu-Oshima eruption, *J. geophys. Res.,* **121,** 2727–2736.

Larsen, R.J. & Marx, M.L., 2012. *An Introduction to Mathematical Statistics and Its Applications,* 5th edn, Pearson.

Maki, M. *et al.*, 2016. Preliminary results of weather radar observations of Sakurajima volcanic smoke, *J. Disaster Res.,* **11,** 15–30.

Marzono, F.S., Barbieri, S., Vulpiani, G. & Rose, W.I., 2006. Volcanic ash cloud retrieval by ground-based microwave weather radar, *IEEE Trans. Geosci. Remote Sens.,* **44,** 3235–3246.

Mastin, L.G. *et al.*, 2009. A multidisciplinary effort to assign realistic source parameters to models of volcanic ash-cloud transport and dispersion during eruptions, *J. Volc. Geotherm. Res.,* **186,** 10–21.

Matoza, R.S. & Fee, D., 2014. Infrasonic component of volcano-seismic eruption tremor. *Geophys. Res. Lett.,* **41,** 1964–1970.

McNutt, S.R., 1994. Volcanic tremor amplitude correlated with eruption explosivity and its potential use in determining ash hazards to aviation, *U.S. Geol. Surv. Bull.,* **2047,** 377–385.

McNutt, S.R., 2004. Volcanic tremor and its use in estimating eruption parameters, in *Proceedings of the 2nd International Conference on Volcanic Ash and Aviation Safety*, Alexandria, Virginia, USA, pp. 49–50, U.S. Department of Commerce NOAA.

McNutt, S.R. & Nishimura, T., 2008. Volcanic tremor during eruptions: temporal characteristics, scaling and constraints on conduit size and processes, *J. Volc. Geotherm. Res.,* **178,** 10–18.

Morioka, H., Kumagai, H. & Maeda, T., 2017. Theoretical basis of the amplitude source location method for volcano-seismic signals, *J. geophys. Res.,* **122,** 6538–6551.

Morton, B.R., Tayler, G. & Turner, J.S., 1956. Turbulent gravitational convection from maintained and instantaneous sources, *Proc. R. Soc. A,* **234,** 1–23.

Mothes, P.A., Yepes, H.A., Hall, M.L., Ramón, P.A., Steele, A.L. & Ruiz, M.C., 2015. The scientific-community interface over the fifteen-year eruptive episode of Tungurahua Volcano, Ecuador, *J. Appl. Volcanol.,* **4,** 9.

Newhall, C.G. & Self, S., 1982. The volcanic explosivity index (VEI) an estimate of explosive magnitude for historical volcanism, *J. geophys. Res.,* **87**(C2), 1231–1238.

Ogiso, M., Matsubayashi, H. & Yamamoto, T., 2015. Descent of tremor source locations before the 2014 phreatic eruption of Ontake volcano, Japan, *Earth Planets Space,* **67,** 206.

Ogiso, M. & Yomogida, K., 2012. Migration of tremor locations before the 2008 eruption of Meakandake volcano, Hokkaido, Japan, *J. Volc. Geotherm. Res.,* **217–218,** 8–20.

Ogiso, M. & Yomogida, K., 2015. Estimation of locations and migration of debris flows on Izu-Oshima Island, Japan, *J. Volc. Geotherm. Res.,* **298,** 15–26.

Prejean, S.G. & Brodsky, E.E., 2011. Volcanic plume height measured by seismic waves based on a mechanical model, *J. geophys. Res.,* **116,** B01306.

Samaniego, P., Pennec, J.L., Robin, C. & Hidalgo, S., 2011. Petrological analysis of the pre-eruptive magmatic process prior to the 2006 explosive eruptions at Tungurahua volcano (Ecuador), *J. Volc. Geotherm. Res.,* **199,** 69–84.

Sato, H., Fehler, M.C. & Maeda, T., 2012. *Seismic Wave Propagation and Scattering in the Heterogeneous Earth,* Springer.

Settle, M., 1978. Volcanic eruption clouds and the thermal power output of explosive eruptions, *J. Volc. Geotherm. Res.,* **3,** 309–324.

Shimbori, T., Sakurai, T., Tahara, M. & Fukui, K., 2013. Observation of eruption clouds with weather radars and meteorological satellites: a case study of the eruptions at Shinmoedake volcano in 2011, *Q. J. Seismol.,* **77,** 139–214.

Sparks, R.S.J., 1986. The dimensions and dynamics of volcanic eruption columns, *Bull. Volcanol.,* **48,** 3–15.

Steffke, A., Fee, D., Garces, M. & Harris, A., 2010. Eruption chronologies, plume heights and eruption styles at Tungurahua Volcano: integrating remote sensing techniques and infrasound, *J. Volc. Geotherm. Res.,* **193,** 143–160.

Suzuki, Y.J., Koyaguchi, T., Ogawa, M. & Hachisu, I., 2005. A numerical study of turbulent mixing in eruption clouds using a three-dimensional fluid dynamics model, *J. geophys. Res.,* **110,** B08201.

Ueda, H., Kozono, T., Fujita, E., Kohno, Y., Nagai, M., Miyagi, Y. & Tanada, T., 2013. Crustal deformation associated with the 2011 Shinmoe-dake eruption as observed by tiltmeters and GPS, *Earth Planets Space,* **65,** 517–525.

Washington Volcanic Ash Advisory Center (VAAC), 2013. Washington VAAC 2013 Volcano Ash Advisory Archive of Tungurahua (July, 14, 2013, 13:42), http://www.ssd.noaa.gov/VAAC/ARCH13/TUNG/2013G141342.html.

Wegler, U., 2003. Analysis of multiple scattering at Vesuvius volcano, Italy, using data of the TomoVes active seismic experiment, *J. Volc. Geotherm. Res.,* **128,** 45–63.

Wilson, L., 1976. Explosive volcanic eruptions—III. Plinian eruption columns, *Geophys. J. Int.,* **45,** 543–556.

Woodhouse, M.J., Hogg, A.J., Phillips, J.C. & Sparks, R.S.J., 2013. Interaction between volcanic plumes and wind during the 2010 Eyjafjallajökull eruption, Iceland, *J. geophys. Res.,* **118,** 92–109.

Woods, A.W., 1988. The fluid dynamics and thermodynamics of eruption columns, *Bull. Volcanol,* **50,** 169–193.

Woulff, G. & McGetchin, T.R., 1976. Acoustic noise from volcanoes: theory and experiment, *Geophys. J. R. astr. Soc.,* **45,** 601–616.

Yamamoto, M. & Sato, H., 2010. Multiple scattering and mode conversion revealed by active seismic experiment at Asama volcano, Japan, *J. geophys. Res.,* **115,** B07304.

APPENDIX: DESCRIPTIONS OF VOLCANIC ACTIVITIES AND ERUPTIONS

We estimated A_s and I_s for eruption tremors and explosion events at Sakurajima, Kuchinoerabujima, Kirishima and Ontake in Japan and Tungurahua in Ecuador (Table 1). Sakurajima hosts two craters, Showa and Minamidake, and repeated Vulcanian eruptions occur at these craters. The eruption on 2013 August 18 was the largest in recent years, producing a plume that reached 5 km above the crater (JMA 2013). In September 2015, many explosive eruptions occurred at the Showa crater after magma intrusion during August 2015 (JMA 2015s). Kuchinoerabujima erupted on 2014 August 3 after a 34-yr repose period, and the explosive phreato-magmatic eruption on 2015 May 29 produced plumes reaching 9 km above the crater and pyroclastic flows on the northwest flank (JMA 2015r). Ontake is the second largest active volcano in Japan, and phreatic eruptions occurred on 2014 September 27 from a vent in Jigokudani, south of the summit. The maximum plume height was 7 km above the vent, and pyroclastic flows occurred (JMA 2014). Kirishima is a volcanic complex consisting of more than 20 volcanic centres, including Shinmoedake and Ohachi, where historical eruptions have mainly occurred. On 2011 January 26–27, sub-Plinian eruptions accompanying Vulcanian eruptions occurred at Shinmoedake (JMA 2011) and were subdivided into three phases (P1–P3; Kozono *et al.* 2014). Eruptive activity at Shinmoedake continued until early September 2011. Tungurahua has produced continued eruptive activity since 1999; major eruptions have produced pyroclastic flows several times since 2006. The 2006 August 16–17 sub-Plinian eruptions generated sizeable pyroclastic flows of 40×10^6 m^3 and plumes reaching 20 km above sea level (Steffke *et al.* 2010; Samaniego *et al.* 2011; Hall *et al.* 2013; Mothes *et al.* 2015).